Air Pressure Data From the Vallée de la Sionne Avalanches of 2004

J. N. McElwaine

Department of Applied Mathematics and Theoretical Physics, University of Cambridge, Cambridge, UK

B. Turnbull

WSL, Swiss Federal Institute for Snow and Avalanche Research, SLF. Davos Dorf, Switzerland

Abstract.
   An air pressure transducer was built into a specially designed housing unit and mounted on the measurement mast of the Vallée de la Sionne avalanche test site in Switzerland. Data from five powder snow avalanches over the winter of 2004 was recorded. An analysis of the sensor response and an interpretation of the signals is given here. The signals are fitted with a simple dipole approximation and the speed and size of each avalanche is estimated. Suggestions for the future development of the sensor are outlined.

1. Introduction

   Despite the death and destruction caused by powder snow avalanches they are poorly understood and there are no satisfactory theories. The main problem in developing models is the lack of high quality, quantitative data. Such data is necessary to give insight into the relevant physical mechanisms so that theories can be developed and validated.

   Powder snow avalanches are gravity currents driven by the increased density of suspended particles. They usually start as a dense granular flow down a slope. As the material accelerates down the slope turbulent eddies in the ambient fluid entrain particles from the upper surface and front, similarly to aeolian saltation. If sufficient material becomes suspended the excess density then provides enough energy to maintain the turbulence and the suspension can flow down the slope as a gravity current.

   Once a powder snow avalanche is developed its dynamics are primarily influenced by its interaction with the ambient air. The interaction with the basal surface is only through deposition and entrainment of snow and is not important dynamically. This suggests that measurements of the air flow, outside and inside an avalanches, would be particularly useful for understanding their dynamics. Conventional sensors for measuring air velocities are hot-wire probes, ultrasonic anemometers and pitot tubes. Hot-wire probes are very fragile and not suitable for use outdoors. Ultrasonic anemometers have been used successfully in front of an avalanche [*Nishimura et al.*, 1989], but they are unreliable inside due to the snow particles and they are easily destroyed. For example *Nishimura et al.* [1993] reports no useful signal. Later work [*Nishimura et al.*, 1995] combined an ultrasonic anemometer with measurements of the static and dynamic air pressure. In one smaller avalanche, the snow density was sufficiently low that the air velocity was successfully measured within the avalanche, however the sensor was subsequently destroyed. Another drawback of ultrasonic anemometers is their low frequency response. The observations of Nishimura used a sensor with a sampling frequency of 20 Hz (current models can operate at up to 100 Hz), which is too low to resolve all the turbulent structure. For these two reasons subsequent work on air flow measurements has focused on pitot type sensors [*Nishimura and Ito*,

1997]. However, the data from these observations is difficult to interpret because of the complex dependence of the measured pressure on the local pressure and velocity and the resonance effects of the instruments. An additional difficulty at Kurobe Canyon is that very little data is available because artificial release is not permitted. Measurements have also been made at the tube-bridge site in Bschlabs, Austria (*Rammer et al.* [1998]), where there were difficulties with low sampling frequency and with the sensor becoming blocked with snow.

   In this paper we describe the results from a new type of air pressure sensor mounted on the measurement mast of the Vallée de la Sionne avalanche test site in Switzerland. We present and analyse data from five powder snow avalanches over the winter of 2004 and conclude with a discussion of an improved sensor design.
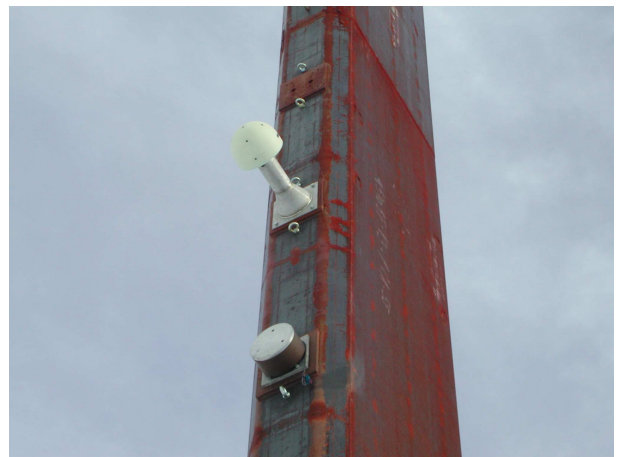
2. Method
2.1. Sensor Design

Figure 1. External view of pressure sensor.

Figure 2. Internal view of pressure sensor. Eight outlets are connected though a junction and moisture trap to a single differential transducer. The other of the transducer is connected to a chamber in the stalk that provides a constant reference pressure.

A pitot type sensor for use in avalanches has to satisfy many requirements. The most interesting place for such a sensor is directly in the path of an avalanche. Since it is too dangerous to venture into such a place when an avalanche may occur the sensor must be installed at the start of the winter. Therefore the sensor must be able to survive harsh mountain conditions over the length of a winter without becoming blocked with snow and also to survive collisions with blocks of ice at more than $50\,\mathrm{ms}^{-1}$.

Nishimura and Ito [1997] used an L-shaped downward pointing metal tube connected by long ($\approx 20\,\mathrm{m}$) plastic tubing to a transducer mounted in an underground bunker at the side of the avalanche track. The use of a downward pointing tube prevented the tube from being blocked by snow and ice, and the location of the transducer in a controlled environment kept it within its operating conditions and prevented it being damaged by water. Though this pioneering work produced useful data there were several drawbacks with this approach. The long length of tubing acts like an organ pipe severely limit the frequency response and introducing unwanted resonances. A tube of $20\,\mathrm{m}$ has a resonance frequency of $330/(4 \times 20) \approx 4\mathrm{Hz}$. Such a peak was indeed found in the power spectrum of the air pressure measurements, but was ascribed to structure in the avalanche. Another difficulty is the complicated flow around an L-shaped tube. The instrument was calibrated for the simplest case of head on air flow. Due to the acceleration of the air round the tube there is a pressure drop at the end and this was found empirically to be $p_o = p_s - 0.44\rho u^2$, where p_o is the pressure at the end of the tube, p_s is the static pressure in the air away from the sensor and u is the air speed. In the Nishimura sensor the pressure was measured relative to the bunker pressure p_b. The measured pressure difference was therefore $\Delta p = p_o - p_b = p_s - p_b - 0.44\rho u^2$. They make the implicit assumption that $p_s = p_b$ so that $\Delta p = -0.44\rho u^2$. This will certainly not be true in general. In particular in front of an avalanche the flow should be irrotational, and assuming steady flow, $p_s + \rho u(u/2 - v) = p_0$ where the constant p_0 is the background atmospheric pressure and v is the avalanche speed. This can be used to eliminate p_s so that $\Delta p = (p_o - p_b) + \rho u(v - 0.94u)$. This indicates the difficulty with this measurement approach. The observations are contaminated by pressure differences in the bunker ($p_o - p_b$) and close to the avalanche front where $u \approx v$ there is heavy cancellation so that $\Delta p \approx (p_o - p_b) + 0.06\rho u^2$. Thus the measured pressure is in fact much more sensitive to changes in the bunker pressure than variations in the air speed.

In a normal pitot probe there are two holes one measuring the stagnation pressure $p_a + 1/2\rho u^2$ and one the static pressure p_s. A differential transducer measures the difference between these two pressures $\Delta p = (p_a + 1/2\rho u^2) - p_a = 1/2\rho u^2$, so it is straightforward to deduce the speed $u = \sqrt{2\Delta p/\rho}$. A difficulty that we have so far avoided mentioning is the directionality of such a sensor. If the air flow is at an angle to the sensor then the pressures are modified. Without additional information or assumptions that specify the angle of the air flow the data cannot be directly interpreted. The solution is to build a sensor with multiple holes so that the full three dimensional velocity can be resolved. This requires at least three transducers, four if the static pressure p_s is also to be resolved. Because of the cost of such transducers, we decided to first build a sensor that would initially only measure the static pressure using one transducer, but could be upgraded in the future to measure the three-component velocity.

Our design is shown in figures 1 and 2. The key features and reasons for the design are as follows.

The sensor is hemispherical in shape so there is a simple analytic solution for the air flow. Thus the effect of the sensor on the pressure can be easily calculated. By averaging the pressure from different points over the surface a good approximation to the static pressure can be obtained that only depends weakly on the air velocity.

To maximise the frequency response the piping between the holes and the transducers should be as short as possible. This is achieved by mounting the transducer directly in the sensor. A large sensor is also robust enough to survive impacts from ice blocks.

To prevent blocking of the holes by ice and snow each hole contains a heated metal pipe. These also help to prevent moisture build up inside the sensor and damage to the transducers. The pipes all then join together and are connected to the transducer through a moisture trap, to provide additional protection.

The sensor is mounted on the mast via a strong metal tube. This is air tight and equalises with the atmospheric pressure p_0 through a valve over a period of tens of minutes. This is used as the reference pressure for the transducer.

The probe was mounted $10\,\mathrm{m}$ from the ground on the $20\,\mathrm{m}$ high mast at the SLF avalanche test site in Vallée de la Sionne in the west of Switzerland. The sensor faces in the approximate direction of the flow and is high enough to be well above any possible dense flowing avalanche. A Kyowa micro-differential pressure transducer and built-in amplifier, PDS-25GA, is used. This is the same basic transducer as used by Nishimura, but with the addition of a built in amplifier, so no signal conditioner is needed. This reduces any electrical interference as the output is low impedance. The transducers were specially calibrated for a low temperature range of $-20°$ C to $+10°$ C. The sensor is rated to $\pm 2,500\,\mathrm{Pa}$ so is suitable for velocities up to $70\,\mathrm{ms}^{-1}$.

The mast is situated at $1600\,\mathrm{m}$ asl and average daily winter temperature was -6.1^o C and sea level adjusted pressure was $102,000\,\mathrm{Pa}$. Using the 1976 standard atmosphere the local air density is estimated as $1.0885\,\mathrm{Kgm}^{-3}$ and the local pressure as $83,444\,\mathrm{Pa}$. The data was sampled at $7,512\,\mathrm{Hz}$ with 12 bits of precision.

2.2. Sensor Response

Here we analyse the response of the transducer to the pressure at the pitot probe. The actual sensor is very complicated. There are eight tubes from each hole connected to a junction box which is then connected through a moisture filter to the transducer (see figure 2). However, to understand the factors that determine the approximate performance of the sensor it is not necessary to model all the

features. To understand the frequency response we consider the system to be a single tube of length $L \approx 0.4\,\mathrm{m}$ diameter $r \approx 2.5\,\mathrm{mm}$ and cross-section $S = \pi r^2$ connected to a cavity of volume $V \approx 2e - 7\,\mathrm{m}^3$ at one end. To model the effect of the sensor on the flow we treat it as a sphere.

2.2.1. Flow Around the Sensor

If the ambient flow field is assumed constant over distances the size of the sensor and is changing slowly then one can consider the whole of a sphere in an ambient fluid with velocity $\mathbf{u}$ and pressure p_0. With $\hat{\mathbf{x}}_i$ the unit vector in the direction of the hole and R the outer radius of the housing, the pressure at a position $R\hat{\mathbf{x}}_i$ on the surface will then be [*Landau and Lifschitz*, 1987]

$$p(\mathbf{x}_i) = p_0 + \rho/8[9(\mathbf{u} \cdot \hat{\mathbf{x}}_i)^2 - 5u^2]. \qquad (1)$$

This will be accurate over parts of the surface where the flow does not separate from the surface. There are eight sensor hole on the sensor connected to the transducer with the following coordinates: $\hat{\mathbf{x}}$, $1/\sqrt{2}(\hat{\mathbf{x}} \pm \hat{\mathbf{y}})$, $1/\sqrt{2}(\hat{\mathbf{x}} \pm \hat{\mathbf{z}})$, $\pm\hat{\mathbf{y}}$ and $-\hat{\mathbf{z}}$. Note that this is not symmetrical since there is no vertical hole as it was felt that this would fill up with snow and water too easily and damage the sensor.

Assuming that the measured pressure will be the average of the pressure at these eight holes the transducer pressure will be

$$p = p_0 - \rho/64[13u^2 + 9(\mathbf{u} \cdot \hat{\mathbf{z}})^2]. \qquad (2)$$

This shows that the measured pressure p will always be lower than the true pressure p_0 and that there is a dependence on the angle of the fluid flow. When the incoming flow is close to the x axis then the pressure will be $p_0 - 13/64\rho u^2$. If the velocity is far from the axis then separation will occur over some of the sensors and the formula will no longer be accurate.

A natural question is what is the best positioning for the holes in order to measure the fluid pressure? This depends on the expected incoming angles of the flow velocity. With the current configuration even small variations in flow angle will cause some of the holes to be in the separation bubble resulting in a noisy signal. By using holes that are closer to the flow direction then a greater range of angles will be effective. Consider 5 holes, one on the x axis and the other four at an angle θ spaced at $90°$ degrees around it. It can be seen from equation 1 that if $\cos\theta = 3/\sqrt{5}$ that is $\theta \approx 42°$ then the pressure at the four offset holes will be p_0. This configuration would give good angle sensitivity if separate transducers were used for each hole. If a single transducer is still to be used to measure the pressure in an averaging configuration choosing $\cos\theta = 2/3$ so that $\theta \approx 48°$ might be a good choice as then for velocity on axis the average pressure is exactly p_0.

3. Results

Table 1. Pressure statistics (all in Pascals) for the different avalanches taken over the whole sequences.

Number	Date	Time	Mean	Std	Min	Max	Median	Interquartile range
6236	2004-01-12	06:28	-27.0	21.4	-176.0	371.5	-31.8	15.9
6237	2004-01-12	10:33	-32.4	10.4	-92.9	89.2	-34.2	1.2
6241	2004-01-13	13.02	-33.8	6.8	-90.4	-1.2	-35.4	6.1
628	2004-01-19	10:35	-34.3	9.4	-129.5	107.5	-35.4	1.2
629	2004-01-19	10:49	-23.2	79.7	-763.7	1867.1	-35.4	6.1

Table 1 shows a remarkably constant zero offset for the sensor of $-35.4\,\mathrm{Pa}$, looking at the median column. This shows that the transducer offset is stable in time and that the pressure equalisation in the support tube is working. In all cases (except 6236) most of the signal is background and the median and interquartile range thus provide a good characterisation of the background zero offset. The quantisation noise is given by

$5 \times 2500/4.995/2^{11} \approx 1.2\,\mathrm{Pa}$, which is equal to the interquartile range for 6237 and 628. This suggests that the sensor and electronics are introducing no appreciable additional noise. The higher values in the three other cases are probably due to background wind registering as small pressure variations, since a $3\,\mathrm{ms}^{-1}$ wind would be expected to produce pressure changes of $\pm 4.5\,\mathrm{Pa}$.
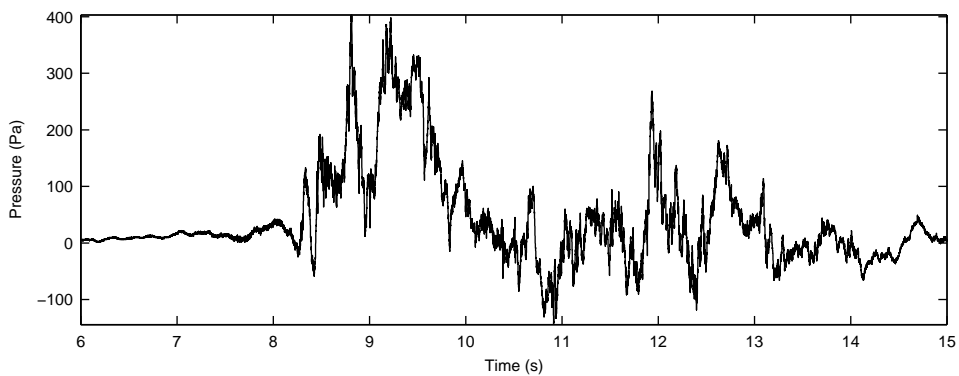
Figure 3. No. 6236. Pressure data during the avalanche
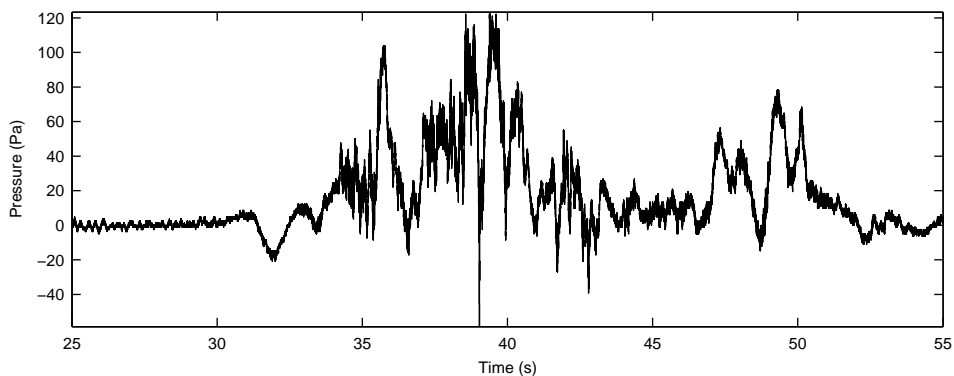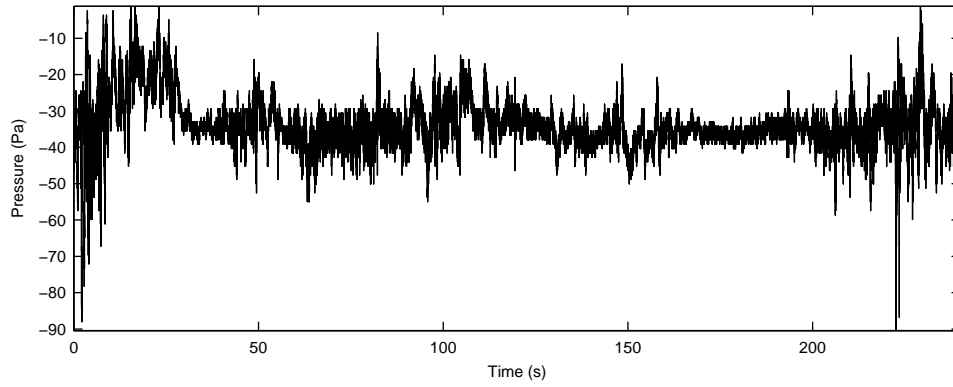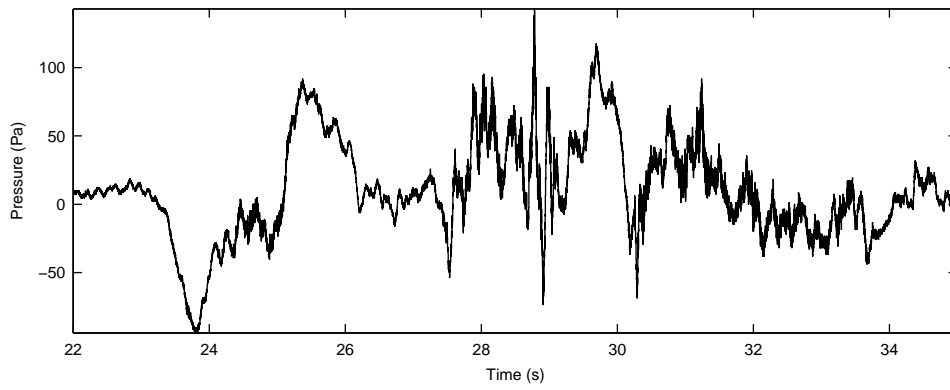

Figure 4. No. 6237. Pressure data during the avalanche

Figure 5. No. 6241. Complete pressure data

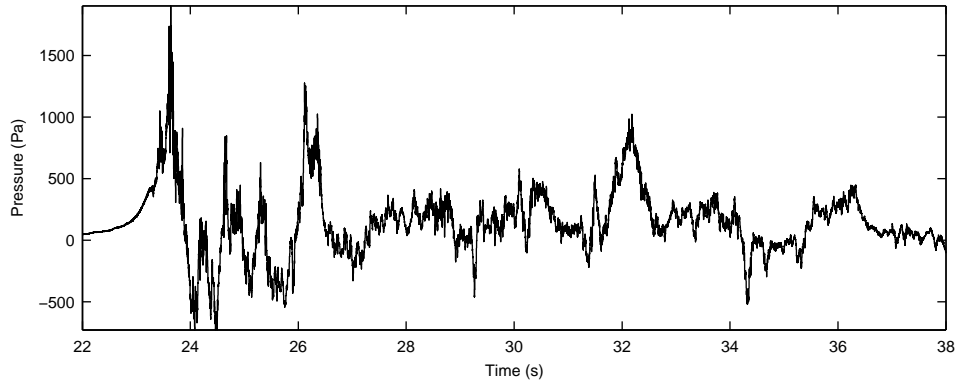**Figure 6.** No. 628. Pressure data during the avalanche

Figure 7. No. 629. Pressure data during the avalanche

3.1. Power Spectra

The power spectrum calculated using Welch's method is shown in figures 8 and 9 for avalanche no. 6236. For all avalanches (unshown) the power spectrum are nearly flat above 1 KHz, though in the largest (no. 629) there is some energy up to 1.5 KHz. Above this frequency there are some identifiable spikes occurring in triples just below 2 KHz and 3 KHz. The natural frequency of the pressure transducer is 1.7 KHz and one of the peaks may be related to this.

The frequency response of the sensor was measured using a signal generator connected via an amplifier to a loud speaker. The frequency of a large amplitude sine wave was varied linearly between 0 and 2000 Hz. The sensor response was recorded. As expected from the complex arrangement of the housing and tubing the frequency response is very complicated. Nevertheless, particular peaks can be identified and agree well with those in the power spectra generated from the avalanche measurements. These peaks are labelled letters A to G in figures 8, 9 and 10.

This procedure demonstrates that measurements at high frequencies are unreliable because of the sensor resonance. Detailed analysis of the fast fluctuations in the turbulent wake is not possible for this data.

Reducing the length of the tubing and removing the moisture trap protecting the sensor are possible ways in which to reduce signal distortion from the resonant frequencies. With a less complicated frequency response it may be possible to apply deconvolution techniques to provide a flat sensor response for measurements. If

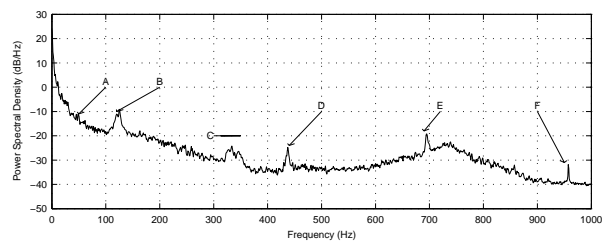successful this would enable the quantitative analysis of the internal turbulent flow.

Figure 8. No. 6236. Power spectral density estimate using Welch method (0-1000 Hz)
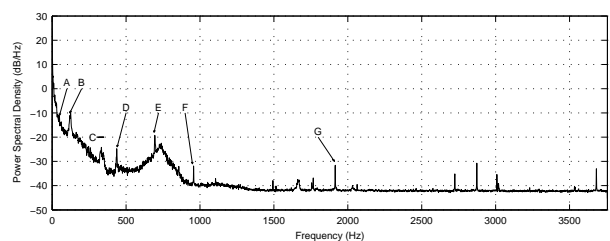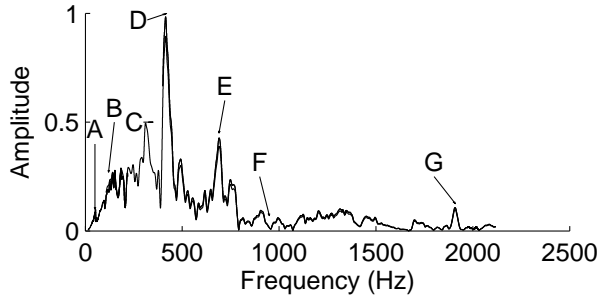

Figure 9. No. 6236. Power spectral density estimate using Welch method (to Nyquist limit)

Figure 10. Frequency response of the sensor measured using a signal generator and loudspeaker. The results of seven experiments are superimposed. Letters A to G label the equivalent peaks in figures 8 and 9.

4. Analysis

4.1. Dipole Approximation

Although in the general case of flow past bodies of arbitrary form the actual flow pattern bears almost no relation to the pattern of potential flow, for *streamlined* shapes the flow may differ very little from potential flow; more precisely, it will be potential flow except in a thin layer of fluid at the surface of the body and in a relatively narrow *wake* behind the body *Landau and Lifschitz* [1987]. In particular in front of the avalanche head the flow will be irrotational since the Reynolds number is very high (for length of 1m, velocity $10 \, \mathrm{ms}^{-1}$, Re $\approx 10^6$). A simple approximation is to assume that the flow field is that of irrotational flow around a sphere where the sphere represents the head of the gravity current in a stationary frame. The flow field has the required symmetries since it is symmetric about the cross-stream $y = 0$ plane and, if the influence of the ground on the air-flow is assumed to be small, the flow field can be reflected in the perpendicular $z = 0$ plane.

A similar approach to the ambient flow around gravity currents was pioneered by *von Kármán* [1940]. He considered the local flow around where the head meets the ground and used this to deduce the head angle 60°. This is accurate over distances small compared to the head height. Similar ideas were also discussed in *Hampton* [1972], but he considered the ambient flow around semi-infinite debris flows, thus his approach is correct over scales large compared to the head height but small compared to the flow length. In contrast the approach in this paper is equivalent to retaining the first three terms (up to the dipole) in a multi-pole expansion and is therefore asymptotically correct.

The pressure for a dipole field in the rest frame of the dipole is (see *McElwaine and Nishimura* [2001] or any fluid dynamics textbook.)

$$p = \frac{\rho u^2 R^3 (3\cos(\theta)^2 - 1)}{2r^3} - \frac{\rho u^2 R^6 (3\cos(\theta)^2 + 1)}{8r^6} \quad (3)$$

where u is the speed and R the effective radius. r and θ are defined by

$$r = \sqrt{L^2 + u^2(t - t_c)^2} \quad (4)$$

$$\cos\theta = \frac{u(t - t_c)}{\sqrt{L^2 + u^2(t - t_c)^2}}, \quad (5)$$

where L is the distance from the centre of the sensor and t_c is the time of closest approach. These four parameters R, u, L and t_c can be found by fitting the observed data. Since the flow will only satisfy eq. 3 where it is irrotational the time of the signal to fit is determined by deciding when the signal becomes turbulent. In general the pressure has a maximum followed by a minimum and then another maximum, but this second maximum will rarely be seen as the flow will have separated and become turbulent. A non-turbulent minimum (corresponding to $t = t_c$) will only be observed if the avalanche passes beneath or to the side of the sensor. When this is the case a stable fit can be obtained for all four parameters, but without the first two turning points the fit is unstable.
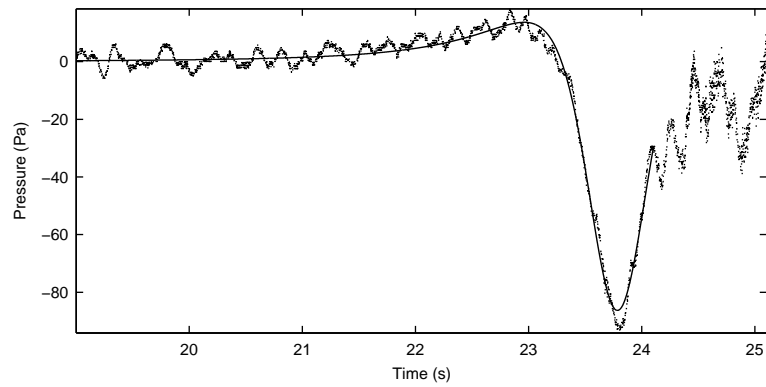
A great difficulty is deciding where the signal changes from the dipole approximation to turbulent flow inside or behind the avalanche. With only one channel of measurement extrapolating the distance from the sensor is ill-conditioned. If pressure data was available from two different positions these difficulties could be dealt with. If extra transducers are present, at least four, then it is no longer necessary, at least in theory, to model the flow at all since the pressure and velocity vector can be calculated from the data.

Recent work [*McElwaine*, 2004] has considered the flow field in the vicinity of the stagnation point. This shows that the front angle should still be 60° on inclines and with internal motion. The calculated pressure distribution (after subtracting of the ambient hydrostatic contribution)

$$p = -\rho r g' \begin{cases} C + \sin\theta_f & \theta \geq \theta_f \\ C + \sin\theta & \theta \leq \theta_f \end{cases}, \quad (6)$$

where g' is the reduced gravity, r and θ polar coordinates, and $\theta_f = \theta_s + \pi/3$ is the angle of the front to the horizontal, and θ_s is the angle of the slope from the horizontal. C is a positive constant that is the ratio of dynamic force to buoyancy forces in the head. Future work is needed to match this solution to the dipole solution and to determine over what region it is valid. The current measurements appear to be too far from the stagnation point to provide good agreement.

4.2. Avalanche no. 628

Figure 11. No. 628. Fitted pressure data near the front

Figure 12. No. 628. The avalanche just before the mast.

The fitted dipole solution is shown in figure 11, where the remarkably good agreement is shown. The dipole solution is strictly valid only for large distances from the avalanche, but the fit suggests that the avalanche is hemispherical to a good approximation. The time for the fit is chosen as about 24.1 s as the flow appears to separate after this and become turbulent. A sensitivity analysis was performed by adding on random Gaussian noise mean zero and standard deviation equal to the residual, and perturbing the initial parameter values for the optimisation by a random factor of ±50 %. The estimated size and offset from the centre agree well with
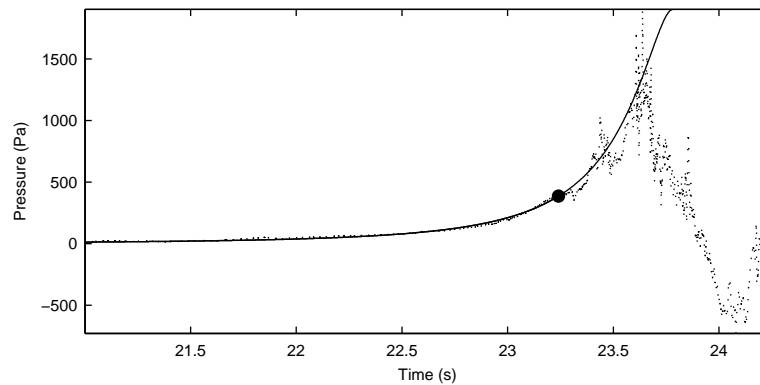
the picture of the avalanche just before it arrives (see figure 12). The calculated dipole velocity also agrees well with the velocity given by the maximum pressure using the air density calculated in section 2.1, (see table 2).

After this the data is much harder to analyse in the turbulent region. There is a large positive oscillation from 24.9–26.2 s. with a peak of 80 Pa ($\approx 12.1\,\mathrm{ms}^{-1}$), which therefore corresponds to a structure of around $(26.2 - 24.9) \times 12.1 = 15.8\,\mathrm{m}$. In line with the other size estimates of structures. The large pressure measurements continue up to around 32 s suggesting that the main section of the avalanche was $(32 - 24) \times 15.8 \approx 120\,\mathrm{m}$. After this time the pressure oscillation vary between $\pm 50\,\mathrm{Pa}$ gradually decaying to background levels at about 70 s. This probably is a turbulent wake with a very low concentration of snow particles.

4.3. Avalanche no. 629

Figure 13. No. 629. Fitted pressure data near the front. Solid line is fit, dashed line is raw data, the solid dot marks the time up to which the data was fitted. Beyond this is extrapolation.
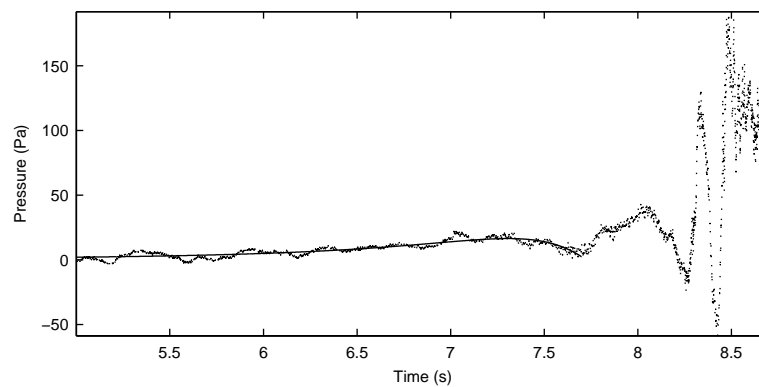
Figure 14. No. 629. The avalanche just before the mast.

Avalanche no. 629 is harder to analyse. Figure 14 shows that the centre of the avalanche is far from the mast. The result of this is that the flow becomes turbulent at the mast before the pressure maximum is reached. This is shown in figure 13. It is still possible to fit the four parameters of the dipole distribution in the same way as for no. 628, but the fit is no longer well conditioned without including the maximum and the decrease afterwards. Instead a three parameter fit of time origin, radius, and offset length is appropriate where the velocity is fixed and given by the velocity of the maximum pressure.
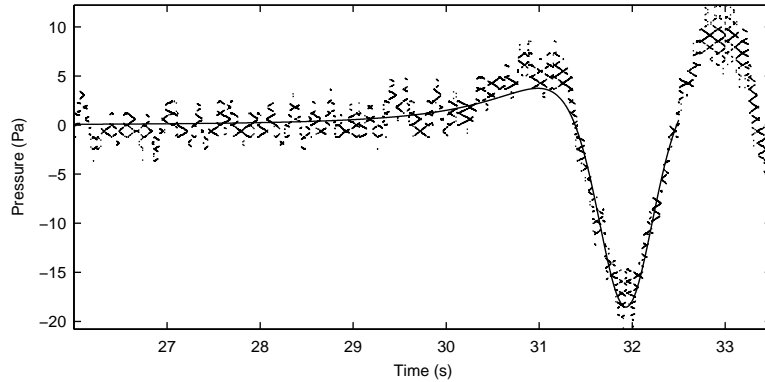
4.4. Avalanche no. 6236

Figure 15. No. 6236. Fitted pressure data near the front

With this avalanche there is very little coherent signal. The pressure sensor is therefore sufficiently far away that it sees little effect of the avalanche until it moves into the turbulent wake. However, if we assume that the first maximum and minimum are the dipole

part then there is a stable fit. There is then a very close agreement between the dipole estimated velocity and the maximum pressure velocity. However the sensitivity analysis shows that this is rather unstable.

4.5. Avalanche no. 6237

Figure 16. No. 6237. Fitted pressure data near the front

Avalanche no. 6237 has only a small signal compared with the turbulent fluctuations in the tail. As for no. 6236 this is because the sensor is far away from the nose of the avalanche and the sensor sees little effect until before it moves into the turbulent wake.
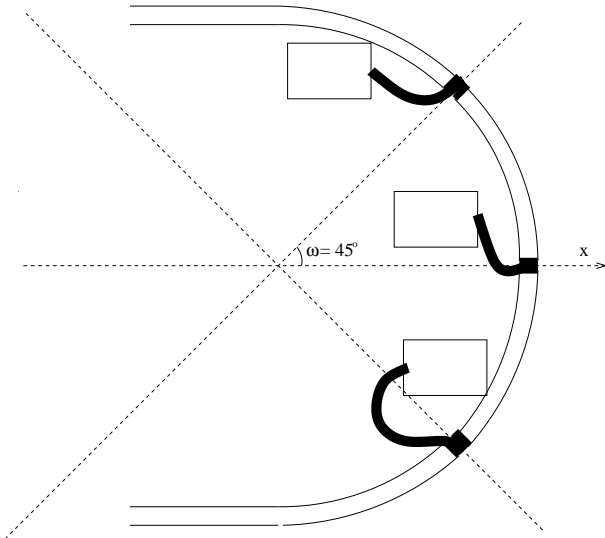
4.6. Avalanche no. 6241

The signal from this avalanche showed no significant features. Photographs of the area show the avalanche was dense and had no powder part. The fluctuations in the signal (figure 5) are disturbances in the ambient air from the passing of the dense flow. No fit has been attempted for this avalanche.

Table 2. Mean fitted parameters with standard deviations calculated by refitting after adding on Gaussian noise with standard deviation of the residual and perturbing the initial choice.

Avalanche	628	629	6236	6237
Max p velocity (m/s)	16.2	59.1	27.2	15.1
Min p velocity (m/s)	13.1	36.6	16.3	10.4
Dipole velocity u(m/s)	15.8 ± 1.0	59.1 ± 0.0	26.4 ± 5.7	69.7 ± 15.5
Dipole radius R(m)	8.2 ± 0.3	28.9 ± 0.0	12.9 ± 0.9	10.3 ± 0.8
Dipole offset L(m)	10.0 ± 0.8	0.0 ± 0.0	21.1 ± 4.7	53.8 ± 12.0
Centre time t_c(m)	23.78 ± 0.00	24.27 ± 0.00	8.32 ± 0.02	31.93 ± 0.00
Residual (Pa)	2.8	9.2	2.6	1.4

5. Design for a Five Hole Sensor

Figure 17. Sketch of the new five hole sensor cross section. The transducers are placed above the height of the inlets, one on the x-axis and four at an of $45°$ from the x-axis.

Now that we have shown that a sensor of this design can survive the winter in Vallée de la Sionne an improved sensor has been designed. Five transducers will be used so that it is possible to estimate the full velocity vector as well as the pressure and also directly estimate the errors. To improve the frequency response the transducers will be mounted as close as possible to the holes as shown in figure 17. By ensuring that the transducers are above the height of the holes it should be possible to prevent them filling with water and be damaged. Any water that collects in the tubes will evaporated by the heating system.

One hole is positioned directly on the sensor axis to measure the stagnation pressure for oncoming flow. The other four are symmetrically positioned at an angle ω from the axis. The choice of this angle is the remaining design decision which we now discuss.

Suppose that the air velocity is
$\mathbf{u} = (\cos\theta, \sin\theta\cos\phi, \sin\theta\sin\phi)$, then the expected pressures will be

$$\hat{P}_0 = p_0 + \tfrac{1}{8}u^2[-5 + 9\cos(\theta)^2]$$
$$\hat{P}_1 = p_0 + \tfrac{1}{8}u^2[-5 + 9(\sin\theta\cos\phi\sin\omega + \cos\omega\cos\theta)^2)]$$
$$\hat{P}_2 = p_0 + \tfrac{1}{8}u^2[-5 + 9(\sin\theta\sin\phi\sin\omega + \cos\omega\cos\theta)^2)]$$
$$\hat{P}_3 = p_0 + \tfrac{1}{8}u^2[-5 + 9(\sin\theta\sin\phi\sin\omega - \cos\omega\cos\theta)^2)]$$
$$\hat{P}_4 = p_0 + \tfrac{1}{8}u^2[-5 + 9(\sin\theta\cos\phi\sin\omega - \cos\omega\cos\theta)^2)].$$
$$(7)$$

The four parameters specifying the fluid flow (p_0, u, θ and ϕ) can then be calculated by minimising

$$L = \sum (p_i - q_i)/(2\sigma^2), \qquad (8)$$

where p_i are the functions given by equations 7 and q_i are the observations. The magnitude of the residual L at the optimal solution gives a measure of the error. A quantitative analysis can be carried out as follows, though only a sketch of the calculation is given here along with the results. The observations q_i are assumed to be exact with the addition of independent identically distributed zero mean Gaussian noise, then minus the log-likelihood is equation 8. After considerable calculation the mean squared errors can be found to be

$$\text{Angle error} = \frac{8\sigma}{9\rho u^2 \sin(2\omega)} \qquad (9)$$

$$\text{Pressure error} = \sigma\frac{\sqrt{29 - 90\cos^2\omega + 81\cos^4\omega}}{9\sin^2\omega} \qquad (10)$$

$$\text{Speed error} = \frac{2\sqrt{5}\sigma}{9\rho u \sin^2\omega}. \qquad (11)$$

This is for the case when the velocity is along the x-axis. For off-axis velocities the expressions are much more complicated. We are mostly interested in velocities close to the axis so we should optimise our sensor for this case. The angle error is minimised with $\omega = 45°$, the pressure error is minimised for $\omega = \tan^{-1}\sqrt{5}/2 = 48°$ and the speed error is minimised for $\theta = 90°$. Note that the pressure minimisation comes at the angle when the pressure estimate is given by the mean of all five holes. However, these calculations are only correct when there is no flow separation over the holes. In order for this to occur all the holes must be in the direction of the flow, thus the smaller ω the wide range of flows can be measured. This suggests that a good compromise is about $45°$. This is close to optimal for calculating the pressure and direction and allows the flow direction to be up to $45°$ off axis before separation will occur near a hole.

6. Conclusions

A new type of air pressure sensor was developed and successfully used in Vallée de la Sionne. This shows that with robust design including heating elements such a sensor can be effective. Where the signal is varying slowly, below the resonance of the instrument, very good agreement with a simple dipole theory is found. This can be used to infer avalanche size, speed and displacement from the sensor. With only one sensor the fit accuracy can be low, demonstrated by avalanche no. 6237. For this avalanche the fitted dipole velocity is very much larger than the maximum pressure prediction. Combining data from sensors at two different locations such as different heights would provide validation of the assumed model and allow further information such as aspect ratio to be calculated and improve the reliability of the analysis.

Inside the avalanche no quantitative analysis has been performed because of the distortion from the instrument resonances, and the complicated turbulent like flow. Without a clear relation between velocity and

pressure, such as the dipole field or wedge flow case, the data is very hard to interpret. This can be dealt with by shortening the tubing connecting the outlets to the transducers to less than 50mm and by installing at least four transducers in each sensor. This will then enable complete resolution of the flow velocity vector and pressure fields at the appropriate frequencies.

References

Hampton, M. A. (1972), The role of subaqueous deris flow in generating turbidity currents, *J. Sed. Pet.*, *42*(4), 775–793.

Landau, L. D., and E. M. Lifschitz (1987), *Fluid Mechanics, Course of Theoretical Physics*, vol. 6, 2nd ed., Butterworth-Heinenann, Oxford.

McElwaine, J. N. (2004), Rotational flow in gravity current heads, *Phil. Trans. R. Soc. Lond.*

McElwaine, J. N., and K. Nishimura (2001), Ping-pong ball avalanche experiments, in *Particulate Gravity Currents*, edited by W. D. McCaffrey, B. C. Kneller, and J. Peakall, no. 31 in Special Publication of the International Association of Sedimentologists, pp. 135–148, Blackwell Science.

Nishimura, K., and Y. Ito (1997), Velocity distribution in snow avalanches, *J. Geophys. Res. B*, *102*(B12), 27,297–27,303, doi: 10.1029/97JB02120.

Nishimura, K., H. Narita, and N. Maeno (1989), The internal structure of powder-snow avalanches, *Ann. Glaciol.*, *13*, 207–210.

Nishimura, K., N. Maeno, F. Sandersen, K. Kristensen, H. Norem, and K. Lied (1993), Observations of the dynamic structure of snow avalanches, *Ann. Glaciol.*, *18*, 313–316.

Nishimura, K., F. Sandersen, K. Kristensen, and K. Lied (1995), Measurements of powder snow avalanche — nature —, *Surv. Geophys.*, *16*, 649–660.

Rammer, L., H. Schaffhauser, and P. Sampl (1998), Computed powder avalanche impact pressures on a tunnel-bridge in ausserfern-tirol, in *Environmental Forest Science, Proceedings of the IUFRO division 8 conference*, edited by K. Sassa, pp. 599–605, Kluwer, Dortrecht.

von Kármán, T. (1940), The engineer grapples with nonlinear problems, *Bull. Am. Math. Soc.*, *46*, 615–683.

J. N. McElwaine †, B. Turnbull,

Swiss Federal Institute for Snow and Avalanche Research, Flüelastrasse 11, CH - 7260 Davos Dorf. Switzerland.

†Permanent address: Department of Applied Mathematics and Theoretical Physics, Centre for Mathematical Sciences, Cambridge University, Wilberforce Road, Cambridge CB3 0WA. UK.